

Suppl. 24, 616 (1968).

⁵R. A. Bryan and B. L. Scott, Phys. Rev. 177, 1435 (1969).

⁶A. E. S. Green and T. Sawada, Rev. Mod. Phys. 39, 594 (1967); Nucl. Phys. B2, 267 (1967).

⁷T. A. Brody and M. Moshinsky, *Tables of Transformation Brackets for Nuclear Shell-Model Calculations* (Dirección General de Publicaciones, Universidad Na-

cional de Mexico, Ciudad Universitaria, Mexico, D. F., 1960).

⁸A. M. Green, Nucl. Phys. 33, 218 (1962).

⁹T. T. S. Kuo and G. E. Brown, Nucl. Phys. 85, 40 (1966).

¹⁰R. A. Arndt, R. Bryan, and M. H. MacGregor, Phys. Letters 21, 314 (1966).

PHYSICAL REVIEW C

VOLUME 6, NUMBER 1

JULY 1972

${}^4\text{He}(e, d)e'{}^2\text{H}$ Angular-Distribution and Cross-Section Measurements Between 36 and 50 MeV

D. M. Skopik*

The American University, Washington, D. C. 20016

and

W. R. Dodge

National Bureau of Standards, Washington, D. C. 20234

(Received 20 March 1972)

Measurements of the angular distributions in the "virtual photon" energy interval of 40 ± 1 MeV and the total cross section in the energy interval of 35.7–49.4 MeV of the ${}^4\text{He}(e, d)e'{}^2\text{H}$ reaction are presented. The data are compared with early calculations and with more recent cluster-model and dispersive calculations.

I. INTRODUCTION

The absorption of photons by the ${}^4\text{He}$ nucleus is predominantly an electric dipole phenomenon. However, in the reaction ${}^4\text{He}(\gamma, d){}^2\text{H}$ both Bose-Einstein statistics in the final state and isospin selection rules for the photodisintegration of a self-conjugate nucleus into two nuclei which are also both self-conjugate forbid the absorption of $E1$ radiation. Furthermore, Bose-Einstein final-state statistics constrain this reaction to proceed only via the absorption of even units of angular momentum. Consequently, the reaction ${}^4\text{He}(\gamma, d){}^2\text{H}$ cannot illuminate the important question of isospin mixing¹ in ${}^4\text{He}$ as could the similar capture reaction ${}^{14}\text{N}(d, \gamma){}^{16}\text{O}$ in ${}^{14}\text{N}$.² Under the usual assumption of a ${}^1\text{S}$ ground state for ${}^4\text{He}$, the lowest-order allowed transition is ${}^1\text{S}$ to ${}^1\text{D}$. The other two allowed transitions (${}^1\text{S}$ to ${}^5\text{S}$ and ${}^1\text{S}$ to ${}^5\text{D}$) both involve the flipping of two nucleon spins and are therefore inhibited by approximately 10^{-3} over the ${}^1\text{S}$ to ${}^1\text{D}$ transition. It is the multipole purity, which is a consequence of identical particles in the final state, and the r^2 weighting of the lowest-order allowed transition which make this reaction important to the study of the four-body system.

We have measured the angular distribution of the ${}^2\text{H}-{}^2\text{H}$ reaction in ${}^4\text{He}$ to ascertain if the angu-

lar distribution is compatible with that expected for an $E2$ transition ($\sin^2 2\theta$). We have also extended previous ${}^2\text{H}(d, \gamma){}^4\text{He}$ measurements³ of the differential cross section at 35 and 135° in the energy interval of 25.8 to 33.3 MeV to 34 and 134° in the energy interval of 35.7 to 49.4 MeV. The National Bureau of Standards (NBS) linear accelerator and the photonuclear physics spectrometer were used for these measurements. Comparison with theory indicates the necessity of including an interaction between the final-state deuterons to obtain a cross section with the observed magnitude. Dispersive-calculation fits to the data below $E_\gamma - Q_{\text{DD}} = 10$ MeV are improved by the assumption of a 2^+ , $T=0$ resonance at 31 ± 2 MeV.⁴

II. EXPERIMENTAL APPARATUS

The major components of the experimental apparatus used to produce an electron beam of well-defined phase space, the NBS linear accelerator⁵ and the electron momentum analyzing system,⁶ have been described previously. In gross features the photonuclear physics spectrometer, which was used in this experiment, is similar to the magnetic spectrometer described by Dodge and Barber⁷ and references contained therein. The spectrometer consists of: (1) a $\frac{2}{3}\pi$ wedge magnet of field in-

dices⁸ $n=0.504$ and $\beta=0.37$ with a rotating-coil gaussmeter for field measurements capable of 0.01% precision ($\Delta H/H$) and a 50-kW stable (0.005% in 4 h) dc power supply; (2) 10 focal-plane semiconductor detectors,⁹ each with a momentum acceptance interval ($\Delta p/p$) of 0.5%; (3) focal-plane detector shielding consisting of a minimum thickness of 60 cm of borax-paraffin, 15.2 cm of Pb, and 5.1 cm of Fe; (4) a ported scattering chamber of 24.1-cm radius with target rotation and translation mechanisms and associated transducers for computer monitoring¹⁰ of target position, temperature, etc.; (5) a turntable on which all of the above components rotate around a vertical axis; (6) absolute and relative incident electron beam current monitors. Of the above spectrometer components, this experiment only depends critically on the performance and calibration of the spectrometer magnet, the focal-plane detector system, and electron beam current monitors.

A ^{210}Po α -particle source was used to obtain a spectrometer energy calibration at 5.303 MeV in the usual way.⁷ The kinetic energy $T_A(i)$ of a particle of mass M_A and charge Z_A incident on the i th focal-plane detector is given as a function of the spectrometer magnetic field H by

$$T_A(i) = M_A \left(\left\{ 1 + \left[\frac{Z_A H P_\alpha}{Z_\alpha H_\alpha(i) M_A} \right]^2 \right\}^{1/2} - 1 \right), \quad (1)$$

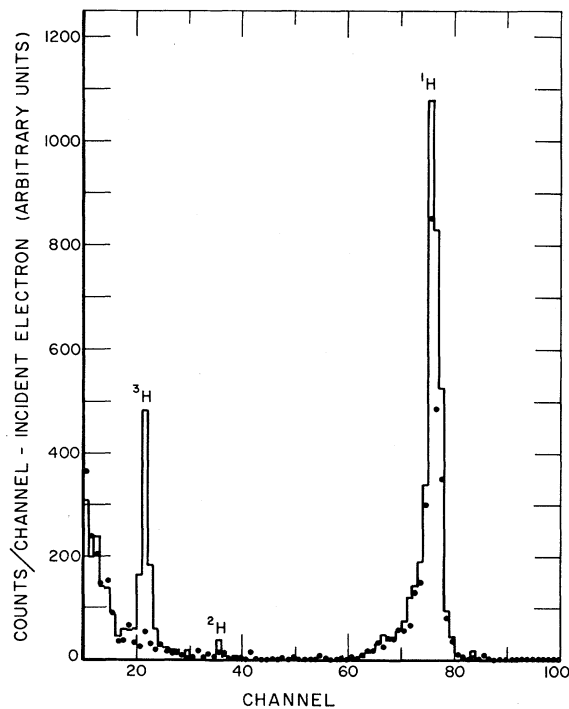


FIG. 1. Signal pulse-height spectrum (histogram) and background pulse-height spectrum (●). Data for $\theta=34^\circ$ and $E_i=41.5$ MeV.

where Z_α is the α -particle charge, M_α is the α -particle mass (taken to be 3727.3 MeV), and $H_\alpha(i)$ is the field required to focus the particular image of the ^{210}Po source on the center of the i th focal-plane detector. To first order $T_A(i)$ is proportional to Z_A^2/M_A , and the energies of ^3H , ^2H , ^4He , and ^3He incident on the i th detector will be in the ratio of $\frac{1}{3}$, $\frac{1}{2}$, 1, and $\frac{4}{3}$ relative to the proton, hence providing the basis for particle mass identification (see Fig. 1).

The spectrometer solid angle $\Delta\Omega$ was measured by rotating a cylindrical shell with apertures of various sizes and shapes around a ^{210}Po α source mounted at the target position in the spectrometer scattering chamber. The spectrometer magnetic field was set at $H_\alpha(i)$ when the i th counter was used to determine $\Delta\Omega$. The α -particle counting rate of the i th focal-plane detector was then measured as a function of the angular position of the shell. The maximum counting rate recorded for several apertures as a function of aperture area is shown in Fig. 2. The slope of the linear least-squares fit to the data of Fig. 2, the aperture-source distance, and the aperture area define the α -source strength S_0 . If the α source emits particles isotropically into the solid angle subtended by the magnet, $\Delta\Omega = C_\alpha/S_0 = 0.0056 \pm 0.0002$, where C_α is the counting rate with the normal magnet en-

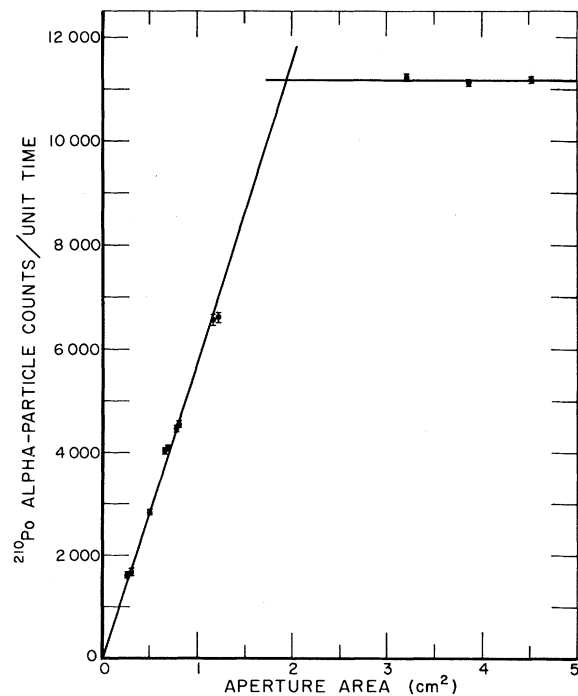


FIG. 2. Measurement of the spectrometer solid angle. The slope of the linear least-squares fit to the data intersecting the origin and the aperture-source distance define the α -particle source strength.

trance apertures in place.

The focal-plane detector system consisted of 10 lithium-compensated $0.1 \times 1.5 \times 6.0$ -cm silicon semiconductor detectors⁹ mounted in the magnet focal plane perpendicular to the incident particle trajectory. The detectors subtended a gross momentum acceptance interval of 7% (including space between the detectors) and a useful momentum acceptance interval of 4.6%. Signals from the focal-plane detectors were amplified by a charge-sensitive preamplifier and single-delay-line amplifier before being fed into 10 gated (gated on approximately 10 μ sec before the 2.7- μ sec-long electron beam pulse) analog-to-digital converters of the Romeo computer system.¹⁰ The relative counting efficiency of the focal-plane detectors was obtained by comparison of the ${}^3\text{H}$, ${}^2\text{H}$, and ${}^1\text{H}$ energy distributions from ${}^4\text{He}$ obtained for each detector. The relative efficiencies were independent of particle energy and charge over the energy region relevant to this experiment. Starting with the highest-energy counter, the relative efficiencies were 1.416, 1.084, 1.042, 1.128, 1.000, 1.026, 1.028, 0.942, and 0.889, all with a standard error of less than 1.5%. The detectors were all maintained at 77°K during an experimental run to ensure the absolute counting efficiency was near 100%.

The bombarding electron energy E_i was determined relative to the spectrometer magnet energy calibration by elastic electron scattering at electron energies which bracketed those used in this experiment. The estimated standard error in E_i was $\pm 1.7\%$. The incident electron energy calibration obtained in this manner was internally consistent, since calculated threshold energies for the reactions ${}^4\text{He}(e, {}^3\text{H})e'p$ and ${}^4\text{He}(e, {}^3\text{He})e'n$ agreed with those observed experimentally. The momentum spread of the incident electron beam, $\pm 1\%$ for this experiment, was fixed by movable slits in the beam-handling system. Typically, the electron beam spot was approximately an ellipse (minor axis = 0.15 cm, major axis = 0.5 cm) with the minor axis vertical.

The absolute beam current was monitored by an induction, "clamp-on ammeter," monitor.¹¹ The response of this monitor relative to a water-cooled "beam dump" was checked periodically. A nonlinearity in the induction monitor preamplifier for beam currents above 22 μA was discovered after completion of this experiment. This nonlinearity introduced an error in beam current measurements made above 22 μA which could have been as high as -10% when the beam current monitor was calibrated at beam currents below 22 μA . Corrections for current monitor nonlinearity were made where necessary.

The ${}^4\text{He}$ gas was contained in a right circular

cylinder of 2.54-cm radius and 5.08-cm height with 0.0008-cm stainless-steel walls.⁷ The axis of the target cell was perpendicular to both the electron beam and deuteron trajectory into the spectrometer magnet. This configuration preserved the mean energy loss of deuterons leaving the cylinder as the spectrometer was rotated about the target axis, but allowed the spectrometer to accept a small fraction of the deuterons produced in the walls at extreme angles. These deuterons from the target cell walls constituted our most deleterious background. The net signal from ${}^4\text{He}$ was obtained by filling the target cell alternately with ${}^4\text{He}$ and ${}^1\text{H}_2$ and by subtracting the ${}^1\text{H}_2$ counts/incident electron from the ${}^4\text{He}$ counts/incident electron. In the worst case the background deuteron counting rate was 4 times the true signal. At 34 and 134° the background deuteron rate was approximately equal to the ${}^4\text{He}(e, d)e'{}^2\text{H}$ rate.

III. CALCULATION OF THE DIFFERENTIAL CROSS SECTION

To avoid confusion which could arise because two identical particles are present in the final state, we define what we will call the differential cross section

$$\left(\frac{d\sigma}{d\Omega}\right)_{\text{lab}} = \frac{C_D}{n_i l(\theta) \Delta\Omega N(E_i, K_0) dK_0/K_0}, \quad (2)$$

where C_D is the number of deuterons of total energy E_D , kinetic energy T_D , and momentum P_D recorded by a counter of momentum acceptance interval $\Delta P_D/P_D$, per incident electron. The spectrometer solid angle is $\Delta\Omega$ and $n_i l(\theta)$ is the number of ${}^4\text{He}$ nuclei/cm² at the spectrometer laboratory angle θ . $N(E_i, K_0) dK_0/K_0$ is the number of real¹² and "virtual" photons per electron in the photon energy interval dK_0 . The "virtual" photon contribution to $N(E_i, K_0) dK_0/K_0$ is defined below. The photon energy interval dK_0 is related to the deuteron momentum interval P_D by

$$\frac{dK_0}{K_0} = \left(\frac{M_{\text{He}}}{M_{\text{He}} T_D + B} + \frac{1 - E_D/P_D \cos\theta}{A - T_D + P_D \cos\theta} \right) \times T_D \frac{T_D + 2M_D}{T_D + M_D} \frac{\Delta P_D}{P_D}. \quad (3)$$

In Eq. (3) $A = M_{\text{He}} - M_D$, $B = Q_{\text{DD}}(A + Q_{\text{DD}}/2)$; M_{He} and M_D are the ${}^4\text{He}$ and the ${}^2\text{H}$ masses, respectively, and Q_{DD} is the ${}^4\text{He}$ - ${}^2\text{H}$ separation energy. The laboratory angle θ and $(d\sigma/d\Omega)_{\text{lab}}$ were transformed to the center-of-mass system by the usual formulas.¹³ Note that we did not divide our deuteron yields by 2. Our definition of the differential cross section for identical particles is consistent with that of Mandl.¹³

A pair of typical signal and background pulse-

height spectra normalized to the same number of incident electrons is shown in Fig. 1. The number of deuteron counts was assumed to be equal to the difference of the two spectra over a visually determined region which extended approximately five channels either side of the deuteron peak. The error in the number of deuteron counts was assumed to be equal to the square root of the sum of the counts in the same region of the two spectra.

The effective target length $l(\theta)$ was determined by numerically integrating the product of the spectrometer transmission function and the electron beam current density over the volume of the target cell. The spectrometer transmission function at 198.9 MeV/c was measured by moving a ^{210}Po α source parallel to the electron beam axis with the spectrometer set at 90° (see Fig. 3). The transmission function was assumed to be the same at all other momenta measured in this experiment. A number of arbitrary current densities were used in computing $l(\theta)$ to determine the sensitivity of $l(\theta)$ to the current density. Some of these greatly exaggerated the possible spatial extent of the electron beam. These calculations showed that uncertainty (standard error) in $l(\theta)$ due to uncertainties in the electron beam current was less than $\pm 2\%$ at all angles. Note that at 90° the transmission function falls entirely within the target cell, and, to second order in the ratio of the electron beam dimensions to the spectrometer magnet effective

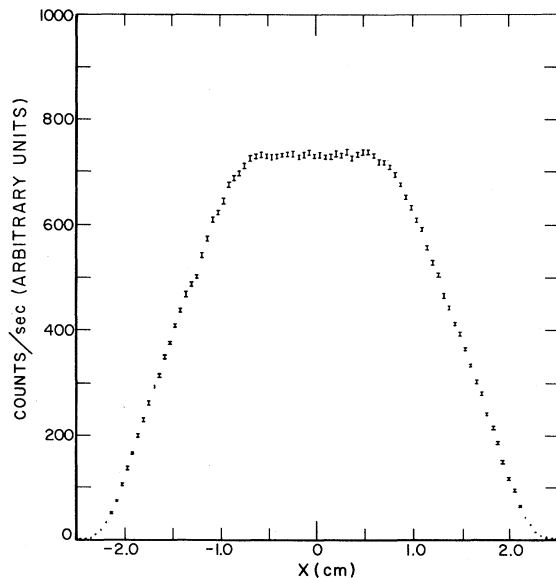


FIG. 3. Relative counting rate of ^{210}Po α particles recorded by a spectrometer focal-plane detector as a function of the perpendicular distance from the central momentum orbit. The source moved on a line through the object (source) position. These data were used in the calculation of the target effective length $l(\theta)$.

radius of curvature, $l(\theta)$ is given by the width of a rectangle of the same height and area as the transmission function.

The pressure and temperature of the ^4He gas were measured at 10-sec intervals by transducers in the gas fill lines and affixed to the target cell bottom, respectively. The averaged values measured during the run were used to compute the number of ^4He nuclei/cm 2 . While the ^4He gas instantaneous temperature was not measured but only the average value, we observed no anomalies in the yield/unit beam current as a function of the beam current. Table I summarizes the errors contributing to $d\sigma/d\Omega$ exclusive of those associated with C_D .

The direct effects of the electron's electromagnetic field (i.e., "virtual photons") and not real photons were used in this experiment,⁷ but because of the way in which the ^2H kinetic energies were programmed, the "virtual photons" which initiated the ^2H - ^2H reaction were nearly on the mass shell (i.e., all attainable values of the three-vector momentum transfer were contained in a cone of half angle $\sim 2.5^\circ$). To compute a cross section we integrated the expressions given by Bosco and Quarati¹⁴ for $d^2\sigma/d\Omega_D d\Omega_e$, over all scattered electron directions. These calculations, which applied only to s -shell nuclei, showed that if the $E2$ photon disintegration cross section were given by

$$\left(\frac{d\sigma}{d\Omega}\right)_\gamma = A(K_\gamma) \sin^2 2\theta_{\text{c.m.}}, \quad (4)$$

the electron disintegration cross section would be

TABLE I. Estimated uncertainties in $(d\sigma/d\Omega)$ exclusive of counting statistics.

Item	Uncertainties in %
I. Incident electron beam current	+2, -10
II. Number of target nuclei	
(a) Target effective length	± 2
(b) Target temperature	+3
(c) Target purity	+1
III. Miscellaneous	
(a) Spectrometer solid angle	± 3.5
(b) Upper limit to real photon contamination from unknown sources.	+4
(c) Uncertainty in number of real and virtual photons due to uncertainty in incident electron energy.	1
	$[\sum (\text{error})^2]^{1/2}$ ± 12

given by

$$\left(\frac{d\sigma}{d\Omega}\right)_e = \frac{\alpha}{\pi} [A(K_0)(N_1^{E2} \sin^2 2\theta_{\text{c.m.}} + N_2^{E2} \sin^2 \theta_{\text{c.m.}} + N_3^{E2}) + B(K_0)(N_1^{E0, E2} \sin^2 \theta_{\text{c.m.}} + N_2^{E0, E2}) + C(K_0)N^{E0}], \quad (5a)$$

where

$$\begin{aligned} N_1^{E2} &= \left[(1+R^2) \ln \frac{2E_i E_f}{mK_0} - \frac{R_K^2}{12} (5R-6)(5R-2) \right], \\ N_2^{E2} &= \frac{1}{12} R_K^2 (2-R^2), \\ N_3^{E2} &= \frac{1}{9} R_K^2 (9-2R+3R^2), \\ N_1^{E0, E2} &= R_K^2 (1-R), \\ N_2^{E0, E2} &= \frac{2}{3} R_K^2 (1+R), \\ N^{E0} &= 4R_K^2, \end{aligned} \quad (5b)$$

and $\theta_{\text{c.m.}}$ is the angle between the detected deuteron and the incident electron in the center-of-mass system, E_i is the total energy of the incident electron, E_f is the total energy of the scattered electron, $R = E_f/E_i$, $R_K = E_f/(E_i - E_f) = E_f/K_0$, and α is the fine-structure constant. Terms labeled by $E2$; $E0, E2$; and $E0$ refer to the pure electric quadrupole, electric monopole-quadrupole interference, and pure monopole transitions as defined in the long wavelength approximation by Bosco and Quarati,¹⁴ and the coefficients $B(K_0)$ and $C(K_0)$ are the squares and products of the corresponding nuclear matrix elements which, of course, are absent in the photodisintegration cross section.¹⁵ The terms multiplied by R_K^2 arise predominantly from the longitudinal components of the electron's transi-

tion field, and their magnitude relative to the leading logarithmic term is a measure of the extent to which this experiment can be directly compared with the photodisintegration experiment. The maximum value of the above ratio in this experiment was ~ 0.003 . Since the initial and final states are orthogonal in a nuclear disintegration, the lowest-order term in the monopole matrix element vanishes and the matrix elements corresponding to $A(K_0)$, $B(K_0)$, and $C(K_0)$ of Eq. (5a) are of the same order in K_0 .¹⁶ Consequently, since the terms N_2^{E2} , N_3^{E2} , $N_1^{E0, E2}$, and N^{E0} of Eq. (5b) are all of order R_K^2 compared to N_1^{E2} , we use $(\alpha/\pi)N_1^{E2}(dK_0/K_0)$ as the number of "virtual" photons in the energy interval dK_0 . Implicit in the integration of $d^2\sigma/d\Omega_D d\Omega_e$, is the assumption that all regions of phase space are accessible to the scattered electron. This is an excellent approximation for the experiment reported here, but may not be, if the detected charged particle is the heavier fragment of a two-body disintegration.

In our experiment we did not detect both deuterons in coincidence, but we programmed the spectrometer magnetic field and the incident electron energy so that only deuterons from the ${}^4\text{He}$ two-body disintegration could be incident on most of our counters in the approximation of forward electron scattering. We show in the Appendix that this approximation is justified by the strong forward peaking of $d^2\sigma/d\Omega_D d\Omega_e$, [using a Born approximation for the energy distribution of deuterons from the reaction ${}^4\text{He}(\gamma, d)p, n$, less than 1% of the deuterons we counted above the two-body threshold could have been produced by the three-body reaction]. In this approximation, deuterons of kinetic

energies greater than

$$T_D = \frac{(K_1 + M_{\text{He}})(K_1 A - C) + K_1^2 M_D \cos^2 \theta + K_1 \cos \theta [(K_1 A - C)^2 + 2M_D(K_1 A - C)(K_1 + M_{\text{He}}) + K_1^2 M_D^2 \cos^2 \theta]^{1/2}}{(K_1 + M_{\text{He}})^2 - K_1^2 \cos^2 \theta} \quad (6)$$

can only be produced by two-body disintegrations. In this expression $K_1 = E_i - m_e$, m_e is the rest energy of the electron, $C = Q_{Dnp}(A + Q_{Dnp}/2)$, Q_{Dnp} is the (${}^4\text{He}; n, p, {}^2\text{H}$) separation energy, and A has been defined previously in Eq. (3).

IV. RESULTS

Figure 4 shows the center-of-mass angular distribution of the reaction ${}^4\text{He}(e, d)e'{}^2\text{H}$ in the energy interval of 40 ± 1 MeV. The high flux of deuterons from the target cell walls precluded measurements at more extreme angles. The measured angular distribution is consistent with $d\sigma/d\Omega$ proportional to $\sin^2 2\theta_{\text{c.m.}}$. Since total cross section refers to the number of events and not the total

number of deuterons,

$$\sigma_T(\gamma, d) = \frac{1}{2} \int_{4\pi} \frac{d\sigma}{d\Omega} d\Omega. \quad (7)$$

Figure 5 shows our total cross-section measurements, together with ${}^2\text{H}(d, \gamma){}^4\text{He}$ measurements, assuming a $\sin^2 2\theta_{\text{c.m.}}$ angular distribution. Values of the total cross section σ_T , shown in Fig. 5, are tabulated in Table II.

If a smooth curve is drawn through the data shown in Fig. 5, then

$$\int_{300}^{\infty} \sigma_{E2} dE = 82 \mu\text{b MeV} \quad (8)$$

and

$$\int_0^{140} (\sigma_{E2}/E^2) dE = 0.066 \mu\text{b}/\text{MeV}. \quad (9)$$

These values can be compared with Quarati's¹⁷ oscillator sum-rule prediction for $\int \sigma_{E2} dE$ (assuming a mean excitation energy of 62 ± 20 MeV) of $5.7_{-3.9}^{+7.5}$ mb MeV and with the $\Delta T = T_z = 0$ sum rule of Gell-Mann and Telegdi¹⁸ for $\int (\sigma_{E2}/E^2) dE = 0.5 \mu\text{b}/\text{MeV}$. It is rather surprising that the ${}^2\text{H}-{}^2\text{H}$ cross section exhausts only 1.4% of the Quarati sum rule, which includes all channels, and only 12.8% of the Gell-Mann-Telegdi sum rule. If we include a lower-limit estimate for $\int \sigma_{E2}(\gamma, p) dE_\gamma$ integrated to 260 MeV of $1700 \mu\text{b MeV}$ obtained from the $E1-E2$ interference terms³ and $\int \sigma_{E2}(\gamma, n) dE_\gamma$ integrated to 140 MeV of $130 \mu\text{b MeV}$,¹⁹ the experimental data satisfy about 33_{-100}^{+25} % of the Quarati $E2$ sum rule.

V. THEORY

Two theoretical calculations of the ${}^4\text{He} + \gamma \rightleftharpoons {}^2\text{H} + {}^2\text{H}$ cross section appeared in the literature before the first experimental measurement. In the earlier calculation, Mandl and Flowers²⁰ used Gaussian wave functions for the ${}^4\text{He}$ and ${}^2\text{H}$ bound states and a plane wave to describe the relative motion of the deuterons (i.e., no final-state interaction). Their calculation is curve 1 in Fig. 5. The use of wave functions which are not eigenfunctions of the same Hamiltonian for the initial and final state and which did not correctly characterize the bound state (such as binding energy and

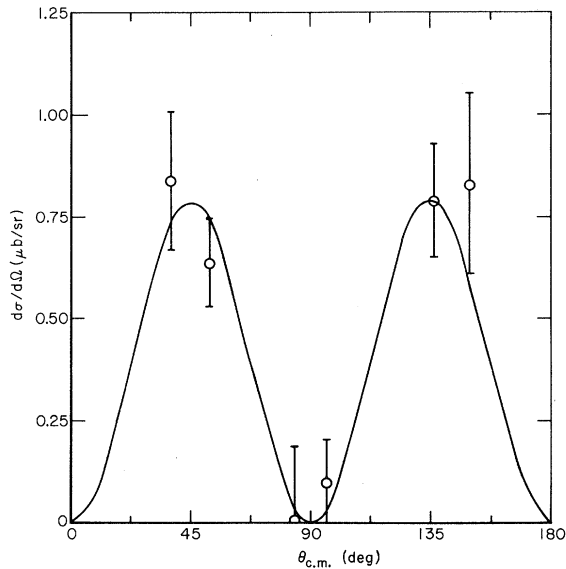


FIG. 4. The ${}^4\text{He}(e, d)e^2\text{H}$ angular distribution in the 40 ± 1 -MeV energy interval. The solid curve is $0.92 \sin^2 2\theta \mu\text{b}/\text{sr}$.

rms charge radius) and the neglect of final-state interactions are among the factors which are responsible for the incorrect magnitude and shape of this calculation. A later coupled-channel calculation by Delves²¹ used data which were derived from the $p + {}^3\text{H} \rightleftharpoons p + {}^3\text{H}$, $n + {}^3\text{He} \rightleftharpoons n + {}^3\text{He}$, ${}^2\text{H} + {}^2\text{H} \rightleftharpoons {}^2\text{H} + {}^2\text{H}$ elastic channels and the $n + {}^3\text{He} \rightleftharpoons p + {}^3\text{H}$, ${}^2\text{H} + {}^2\text{H} \rightleftharpoons p + {}^3\text{H}$, $n + {}^3\text{He}$ inelastic channels to estimate the amount of low-energy s -wave ${}^2\text{H}-{}^2\text{H}$ clustering in ${}^4\text{He}$. The ${}^2\text{H}-{}^2\text{H}$ clustering estimate was then used to calculate the capture cross section. This cross section has a maximum value of $2 \times 10^{-33} \text{ cm}^2$ at a deuteron laboratory energy of 40 MeV, corresponding to a maximum $\sigma(\gamma, d)$ of $0.1 \mu\text{b}$ at 43 MeV. However, it is not clear

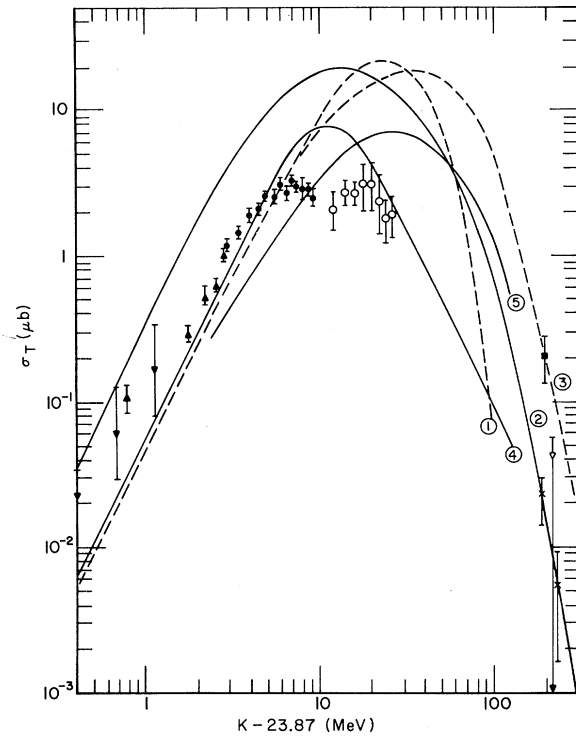


FIG. 5. The ${}^4\text{He}(\gamma, d){}^2\text{H}$ total cross section. The data shown here are: \circ , this measurement; \bullet , Meyerhof, *et al.* (Ref. 3); ∇ , Zurmühle, Stephens, and Staub (Ref. 22); \blacktriangle , A. Degré, M. Schaeffer, and M. Suffert, private communication to W. E. Meyerhof (Ref. 3); ∇ , J. A. Poirier and M. Pripstein, *Phys. Rev.* **130**, 1171 (1963); \times , Asbury and Loeffler (Ref. 23); \blacksquare , Yu. K. Akimov, O. V. Savchenko, and M. L. Soroko, *Zh. Eksperim. i Teor. Fiz.* **41**, 708 (1961) [transl.: *Soviet Phys.-JETP* **14**, 512 (1962)]. Curve 1 is calculated from expressions in Mandl and Flowers (Ref. 20); curve 2 is from Asbury and Loeffler (Ref. 23); curve 3 is from Ahmed, Chowdhury, and Husain (Ref. 24); curve 4 is from Thompson (Ref. 25) for an exchange-mixture parameter $\gamma = 1.5$; curve 5 is from Thompson (Ref. 25) with the same ${}^4\text{He}$ and ${}^2\text{H}$ wave functions as curve 4 but no final-state interaction.

TABLE II. All ${}^4\text{He} + \gamma \rightleftharpoons {}^2\text{H} + {}^2\text{H}$ data published up to August 1971 plus the unpublished data of Degré. Uncertainties are those quoted by the original authors. All data are referred to the absorption experiment ${}^4\text{He} + \gamma \rightarrow {}^2\text{H} + {}^2\text{H}$ in the center-of-mass system. The production experiment $d\sigma/d\Omega$ and σ_T has been converted to the absorption experiment by

$$\frac{d\sigma}{d\Omega}(\gamma, d) = \frac{9}{2} \left(\frac{P_d}{K_\gamma} \right)^2 \frac{d\sigma}{d\Omega}(d, \gamma) \quad \text{and} \quad \sigma(\gamma, d) = \frac{9}{4} \left(\frac{P_d}{K_\gamma} \right)^2 \sigma(d, \gamma).$$

$E_\gamma - Q$ (MeV)	$\theta_{\text{c.m.}}$ (deg)	$d\sigma/d\Omega$ ($\mu\text{b}/\text{sr}$)	σ_T (μb)	Experiment
190.7	41.5	0.119 \pm 0.044	0.202 \pm 0.076	Production ^a
215.7	65	\leq 0.0078 \pm 0.002	\leq 0.044 \pm 0.012	Production ^b
184.6	52.4	0.0063 \pm 0.0022	0.022 \pm 0.008	Absorption ^c
224.4	53.2	0.0015 \pm 0.0011	0.0054 \pm 0.0038	Absorption ^c
0.32	45.6	...	0.023	Production ^d
0.60	45.8	0.018 $^{+0.036}_{-0.030}$	0.061 $^{+0.122}_{-0.030}$	Production ^d
1.04	46	...	0.17	Production ^d
1.91	131.3	0.175 \pm 0.079	0.59 \pm 0.27	Production ^e
2.90	131.6	0.378 \pm 0.095	1.32 \pm 0.33	Production ^e
3.89	131.9	0.644 \pm 0.071	2.26 \pm 0.25	Production ^e
4.88	132.2	0.842 \pm 0.035	2.83 \pm 0.12	Production ^e
2.88	136.6	0.351 \pm 0.036	1.18 \pm 0.12	Production ^f
3.39	136.8	0.432 \pm 0.036	1.45 \pm 0.12	Production ^f
3.89	136.9	0.566 \pm 0.063	1.90 \pm 0.21	Production ^f
4.40	137	0.608 \pm 0.064	2.06 \pm 0.22	Production ^f
4.91	137.1	0.628 \pm 0.030	2.54 \pm 0.12	Production ^f
5.41	137.3	0.729 \pm 0.085	2.48 \pm 0.29	Production ^f
5.91	137.4	0.894 \pm 0.112	3.04 \pm 0.38	Production ^f
6.42	137.5	0.782 \pm 0.094	2.66 \pm 0.32	Production ^f
6.92	137.6	0.966 \pm 0.070	3.29 \pm 0.24	Production ^f
7.42	137.7	0.863 \pm 0.068	2.94 \pm 0.23	Production ^f
7.93	137.8	0.827 \pm 0.076	2.82 \pm 0.26	Production ^f
8.43	137.8	0.903 \pm 0.100	3.08 \pm 0.34	Production ^f
8.93	137.9	0.820 \pm 0.094	2.80 \pm 0.32	Production ^f
9.43	138	0.726 \pm 0.114	2.48 \pm 0.39	Production ^f
15.9	38	0.84 \pm 0.18	3.0 \pm 0.6	${}^4\text{He} + e \rightarrow {}^2\text{H} + {}^2\text{H} + e' \text{ }^g$
15.9	53	0.65 \pm 0.15	2.4 \pm 0.5	${}^4\text{He} + e \rightarrow {}^2\text{H} + {}^2\text{H} + e' \text{ }^g$
15.9	83	0.01 \pm 0.10	...	${}^4\text{He} + e \rightarrow {}^2\text{H} + {}^2\text{H} + e' \text{ }^g$
15.9	97	0.10 \pm 0.10	...	${}^4\text{He} + e \rightarrow {}^2\text{H} + {}^2\text{H} + e' \text{ }^g$
15.9	137	0.80 \pm 0.14	2.7 \pm 0.5	${}^4\text{He} + e \rightarrow {}^2\text{H} + {}^2\text{H} + e' \text{ }^g$
15.9	152	0.83 \pm 0.22	4.2 \pm 1.1	${}^4\text{He} + e \rightarrow {}^2\text{H} + {}^2\text{H} + e' \text{ }^g$
11.8	37	0.58 \pm 0.16	2.1 \pm 0.6	${}^4\text{He} + e \rightarrow {}^2\text{H} + {}^2\text{H} + e' \text{ }^g$
13.7	38	0.63 \pm 0.11	2.7 \pm 0.5	${}^4\text{He} + e \rightarrow {}^2\text{H} + {}^2\text{H} + e' \text{ }^g$
17.6	152	0.60 \pm 0.20	3.1 \pm 1.1	${}^4\text{He} + e \rightarrow {}^2\text{H} + {}^2\text{H} + e' \text{ }^g$
19.6	152	0.60 \pm 0.20	3.1 \pm 1.1	${}^4\text{He} + e \rightarrow {}^2\text{H} + {}^2\text{H} + e' \text{ }^g$
21.5	153	0.46 \pm 0.20	2.5 \pm 1.1	${}^4\text{He} + e \rightarrow {}^2\text{H} + {}^2\text{H} + e' \text{ }^g$
23.5	154	0.32 \pm 0.10	1.8 \pm 0.6	${}^4\text{He} + e \rightarrow {}^2\text{H} + {}^2\text{H} + e' \text{ }^g$
25.5	154	0.33 \pm 0.10	1.9 \pm 0.6	${}^4\text{He} + e \rightarrow {}^2\text{H} + {}^2\text{H} + e' \text{ }^g$
0.80	0.112 \pm 0.026	Production ^h
1.30	0.303 \pm 0.044	Production ^h
1.80	0.577 \pm 0.084	Production ^h
2.30	0.766 \pm 0.111	Production ^h
2.80	1.005 \pm 0.093	Production ^h

^aYu. K. Akimov, O. V. Savchenko, and M. L. Soroko, Zh. Eksperim. i Teor. Fiz. **41**, 708 (1961) [transl.: Soviet Phys.-JETP **14**, 512 (1962)].

^bJ. A. Poirier and M. Pripstein, Phys. Rev. **130**, 1171 (1963).

^cSee Ref. 23.

^dSee Ref. 22.

^eW. Del Bianco and J. M. Poutissou, Phys. Letters **29B**, 299 (1969).

^fSee Ref. 3.

^gThis experiment. Uncertainties are due to counting statistics only.

^hA. Degré, M. Schaeffer, and M. Suffert, private communication to W. E. Meyerhof (Ref. 3).

that the s -wave clustering of ${}^2\text{H}$ - ${}^2\text{H}$ in the ground state of ${}^4\text{He}$ is directly related to the d -wave ${}^2\text{H}$ - ${}^2\text{H}$ breakup of ${}^4\text{He}$ as Delves²¹ assumed.

Since the advent of the first experimental data of Zurmühle, Stephens, and Staub²² below pion thresholds, four additional calculations have been made. Asbury and Loeffler²³ used an exponential ${}^4\text{He}$ wave function to fit both the Zurmühle, Stephens, and Staub data and their ${}^4\text{He}(\gamma, d)$ experimental data at 185 and 224 MeV. However, their fit (curve 2 in Fig. 5) with a simple $E2$ operator is not necessarily meaningful at energies close to and above the pion thresholds. The calculation of Ahmed, Chowdhury, and Husain²⁴ used a Hulthén ${}^4\text{He}$ ground-state wave function, a Yukawa deuteron wave function, and no final-state interaction (plane-wave function for the deuteron relative motion). Their ${}^4\text{He}$ wave function reproduced the correct binding energy and charge radius. Their calculation is curve 3 in Fig. 5.

All calculations described above, except Delves's,²¹ share the common defect of predicting a peak cross section approximately an order of mag-

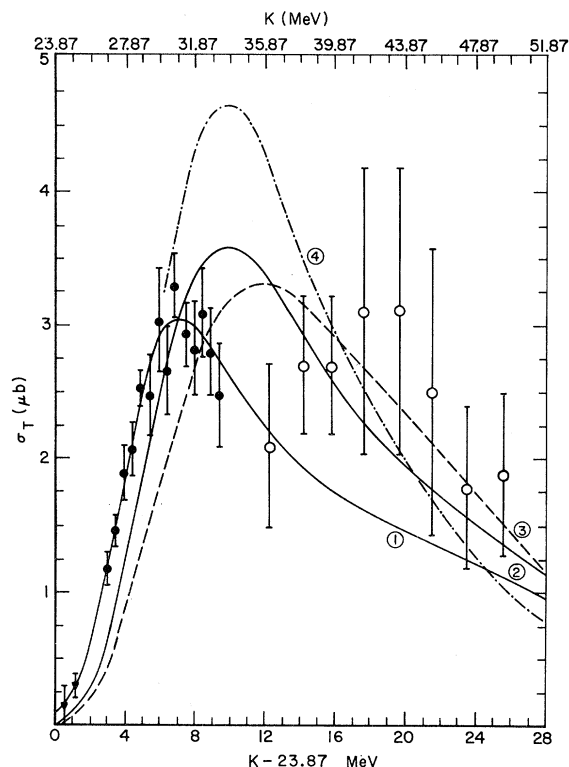


FIG. 6. The ${}^4\text{He}(\gamma, d){}^2\text{H}$ total cross section with the same notation as Fig. 5. Curve 1 is from Erdas *et al.* (Ref. 4) with resonance parameters $E_{ex} = 33$ MeV and a reduced width of 5 MeV. Curve 2 is from Erdas *et al.* (Ref. 4) with $E_{ex} = 30$ MeV and a reduced width of 3.2 MeV. Curves 3 and 4 are from Gibson (Ref. 26) with $V_a = 210$ and 230 MeV.

nitude too large. Thompson²⁵ calculated the ${}^4\text{He}(\gamma, {}^2\text{H}){}^2\text{H}$ cross section using the 1D_2 part of the wave function he derived to describe ${}^2\text{H}$ - ${}^2\text{H}$ elastic scattering data. These wave functions were cal-

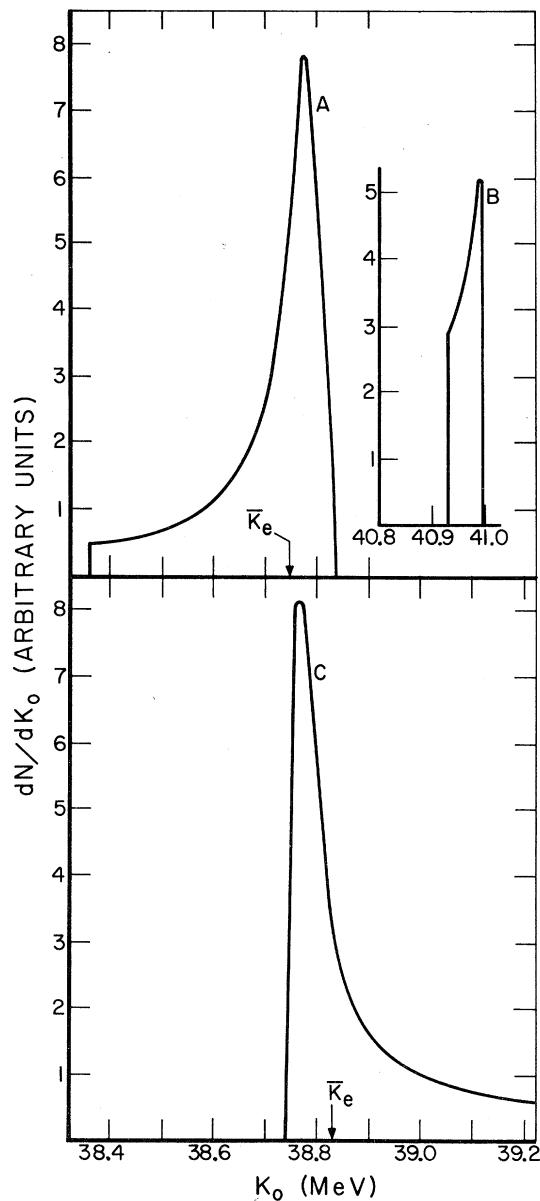


FIG. 7. The differential virtual-photon intensity spectrum $dN(E_i, K_0)/dK_0$. All curves are for $E_i = 41.511$ MeV. Curves A and C give the differential intensity spectrum relevant to the production of 8.870-MeV deuterons at 34° and 5.907-MeV deuterons at 146° from the reaction ${}^4\text{He} + e \rightleftharpoons {}^2\text{H} + {}^2\text{H} + e$. These are the maximum energies which deuterons from the reaction ${}^4\text{He} + \gamma \rightleftharpoons {}^2\text{H} + n + p$ can have at the indicated angles and $E_i = 41.511$ MeV. Curve B gives $dN(E_i, K_0)/dK_0$ for the reaction ${}^4\text{He} + e \rightleftharpoons {}^2\text{H} + n + p + e'$ for the same deuteron energy and angle as in curve A. \bar{K}_0 is the mean energy transfer in electrodisintegration. See the Appendix for details.

culated using the resonating-group-structure approximation.²⁵ In the approximations of his model specific distortion effects other than exchange effects are neglected. He uses a superposition of two Gaussian wave functions to describe the deuteron clusters and essentially a distorted plane wave to describe the deuteron relative motion. Thompson²⁵ made two assumptions for the initial state, a Gaussian and an Irving-Gunn wave function, both of which reproduced the correct charge radius. The relative-motion wave function was determined by minimizing the total energy of the ${}^2\text{H}$ - ${}^2\text{H}$ system. The two-nucleon potential he used contained an exchange mixture parametrized by γ . The ${}^2\text{H}$ - ${}^2\text{H}$ elastic scattering data restricted γ to values between 1 and 1.5. He concluded that both final-state interactions and an Irving-Gunn wave function for ${}^4\text{He}$ were necessary to fit the data (curve 4, Fig. 5). We surmised from Thompson's calculation with no final-state interaction (curve 5, Fig. 5) that use of a two-term Gaussian wave function to describe the spatial behavior of the deuterons reduced the maximum value of the cross section by a factor of 4 over the calculations of Asbury and Loeffler²³ and Ahmed, Chowdhury, and Husain.²⁴ Since the final-state interaction was basically attractive, the effect of the final-state interactions quite reasonably was to enhance the lower-energy region of the cross section, while denuding the high-energy region somewhat. However, Gibson²⁶ has shown that a Born-approximation calculation using Jacobi coordinates, Thompson's²⁵ initial state, and Hulthén wave functions for the deuterons yields a peak cross section in agreement with Asbury and Loeffler²³ and Ahmed, Chowdhury, and Husain.²⁴ Gibson²⁶ concluded that the factor of 4 in absolute magnitude between Thompson's²⁵ and other plane-wave calculations^{23,24,26} was due to an error in the former's calculation.

Erdas *et al.*⁴ have used a dispersive approach to this problem. Their method assumes that the matrix element for the reaction ${}^4\text{He}(\gamma, {}^2\text{H}){}^2\text{H}$ is known

if the elastic phase shifts of the ${}^2\text{H}$ - ${}^2\text{H}$ system are known over all positive energies. The initial- and final-state wave functions are taken to be Gaussians with free parameters adjusted to reproduce the ${}^4\text{He}$ and ${}^2\text{H}$ matter radii. Since experimental phase shifts do not exist or are poorly determined, Erdas *et al.*⁴ assumed the phase shifts are given by a hard sphere plus a $T=0$, 2^+ resonance. The presence of a $T=0$, 2^+ resonance above the ${}^4\text{He}$ four-body threshold has been implied in the ${}^2\text{H}$ - ${}^2\text{H}$ elastic scattering data.²⁷ The cross-section peak energy and magnitude are in good agreement with experiment (Fig. 6; σ_T calculated for resonance excitation energies of 30 and 33 MeV and reduced width of 5 MeV are essentially the same). The broad maximum above 33 MeV is due to the use of a hard-sphere phase shift.

Gibson²⁶ has made a single-channel calculation with the initial and final states described above and with the ${}^2\text{H}$ - ${}^2\text{H}$ relative-motion wave function calculated numerically from the Schrödinger equation. He used a potential of the Volkov²⁸ form

$$V(r) = -V_a e^{-r^2/a^2} + V_0 e^{-r^2/\rho^2}, \quad (10)$$

where r is the relative coordinate of the two deuterons, to describe the ${}^2\text{H}$ - ${}^2\text{H}$ interaction. Curves 3 and 4, Fig. 6, are Gibson's²⁶ calculations obtained using $V_a = 210$ and 230 MeV, $V_0 = 200$ MeV, $a = 2.1$ F, and $\rho = 1.0$ F. Gibson stated that the strongly repulsive, short-range potential was necessary to simulate the effect of the other open channels.

VI. CONCLUSIONS

Our experiment is consistent with an $E2$ multipolarity assignment for the reaction ${}^4\text{He}(\gamma, d){}^2\text{H}$ and with the lower-energy data of Meyerhof *et al.*³ The necessity of the inclusion of final-state interactions seems well established by the calculations of Thompson,²⁵ Erdas *et al.*,⁴ and Gibson,²⁶ while the need for a $T=0$, 2^+ resonance at 31 ± 2 MeV seems somewhat less well established.

APPENDIX

The correct expression for the energy transfer in an electron disintegration is given by

$$K_0 = \frac{M_{\text{He}} T_D + Q_{\text{DD}}(M_{\text{He}} - M_D + Q_{\text{DD}}/2) + E_i P_D (\cos \theta_{e'D} - \cos \theta_{eD}) + 2E_i^2 \sin^2(\theta_{ee'}/2)}{M_{\text{He}} - M_D - T_D + P_D \cos \theta_{e'D} + 2E_i \sin^2(\theta_{ee'}/2)}, \quad (11)$$

where θ_{eD} , $\theta_{e'D}$ are the angles between the initial and scattered electron and the detected deuteron, and the other symbols have been previously defined. We measured only the momentum and energy of a deuteron from the electrodisintegration of

${}^4\text{He}$. In the reaction ${}^4\text{He} + \gamma \rightleftharpoons {}^2\text{H} + {}^2\text{H}$ measurement of the ${}^2\text{H}$ momentum is sufficient to determine the energy of the absorbed real photon; however, in the reaction ${}^4\text{He} + e \rightleftharpoons {}^2\text{H} + {}^2\text{H} + e'$ measurement of the ${}^2\text{H}$ momentum alone is not sufficient to deter-

mine the energy of the absorbed virtual photon. Hence, the deuterons we measured from ${}^4\text{He} + e \rightleftharpoons {}^2\text{H} + {}^2\text{H} + e'$ were produced by a distribution of virtual-photon energies centered around the real-photon energy transfer. In Fig. 7 we plot

$$\frac{dN(E_i, K_0)}{dK_0} = \frac{1}{A(K_0)} \int_{\theta_e} \frac{d^2\sigma}{d\Omega_p d\Omega_e} \frac{d\varphi_e'}{dK_0} d(\cos\theta_e'), \quad (12)$$

where $N(E_i, K_0)$ is the virtual-photon intensity spectrum for $E_i = 41.511$ MeV with $T_D = 8.870$ MeV, $\theta_{eD} = 34^\circ$ (curve A); and with $T_D = 5.907$ MeV, $\theta_{eD} = 146^\circ$ (curve C).²⁹ Equation (12) is most conveniently evaluated in a coordinate system with the polar axis in the direction of \vec{P}_D or \vec{P}_e . We choose the polar axis in the direction of \vec{P}_e . The $d\varphi_e'/dK_0$ is defined by

$$\cos\theta_{e'D} = \cos\theta_e \cos\theta_D + \sin\theta_e \sin\theta_D \cos(\varphi_e' - \varphi_D) \quad (13)$$

and Eq. (11). Here (θ_e, φ_e') and (θ_D, φ_D) are the (polar, azimuthal) angles of the scattered electron and emitted deuteron. $A(K_0)$ is defined in Eq. (5). $B(K_0)$ and $C(K_0)$ in Eq. (5) were neglected. These

curves show the behavior of $dN(E_i, K_0)/dK_0$ as a function of the detected deuteron angle. In Fig. 7 (curve B) we plot $dN(E_i, K_0)/dK_0$ for the reaction ${}^4\text{He} + e' \rightleftharpoons {}^2\text{H} + n + p + e'$. We assumed the deuteron had the same [and the (n, p) pair the opposite] momentum as in curve A. In the reaction ${}^4\text{He} + \gamma \rightleftharpoons {}^2\text{H} + n + p$ a deuteron of this momentum would correspond to the absorption of a 41-MeV photon and hence would not occur. Using the Born approximation to calculate the energy distribution of deuterons in the three-body breakup (the Born approximation is in reasonable agreement with the data of Gorbunov and Spiridonov³⁰), we conclude that an upper limit for the fraction of deuterons from the three-body breakup included in our yield from this effect is $<1\%$.

ACKNOWLEDGMENT

We wish to thank Dr. D. R. Lehman, Dr. E. G. Fuller, Dr. E. V. Hayward, and Dr. B. F. Gibson for many helpful and informative discussions. Dr. J. J. Murphy, II, assisted in all phases of the experiment and we wish to extend to him our especial thanks. The help of the NBS linac crew is gratefully acknowledged.

*U. S. Atomic Energy Commission Fellow at National Bureau of Standards; now at University of Saskatchewan, Saskatoon, Canada.

¹B. L. Berman, S. C. Fultz, and M. A. Kelly, Phys. Rev. C **4**, 723 (1971).

²M. Suffert, G. Costa, D. Magnac-Valette, in *Proceedings of the Conference on Direct Interactions and Nuclear Reaction Mechanisms, Padua, Italy, 1962*, edited by E. Clementel and C. Villi (Gordon and Breach, New York, 1963) p. 842; J. Phys. **24**, 1029 (1963); M. Suffert, Nucl. Phys. **75**, 226 (1966).

³W. E. Meyerhof, W. Feldman, S. Gilbert, and W. O'Connell, Nucl. Phys. **A131**, 489 (1969).

⁴F. Erdas, A. Pompei, P. Quarati, and B. Mosconi, private communication to W. R. Dodge. The remark of Ref. 25 applies to this reference.

⁵J. E. Leiss, in *Proceedings of the 1966 Linear Accelerator Conference, October 3-7, 1966*, (Los Alamos Scientific Laboratory of the University of California, Los Alamos, New Mexico) p. 20.

⁶S. Penner, Rev. Sci. Instr. **32**, 150 (1961); **32**, 1068 (1961).

⁷W. R. Dodge and W. C. Barber, Phys. Rev. **127**, 1746 (1962).

⁸K. Brown, private communication to W. R. Dodge. Here $n = (r/H) (\partial H / \partial r)|_{r=r_0}$ and $\beta = (r/H)^2 (\partial^2 H / \partial r^2)|_{r=r_0}$ where r_0 is the central momentum orbit.

⁹W. R. Dodge, J. A. Coleman, and S. R. Domen, Rev. Sci. Instr. **37**, 1151 (1966); W. R. Dodge, J. A. Coleman, and S. R. Domen, Nucl. Instr. Methods **42**, 181 (1966).

¹⁰J. Broberg, J. E. Leiss, R. A. Schrack, and J. M. Wyckoff, IEEE Trans. Nucl. Sci. **NS-11**, 331 (1964).

¹¹L. Bess and A. O. Hansen, Rev. Sci. Instr. **19**, 108 (1948); L. Bess, J. Ovadia, and J. Valassis, *ibid.* **30**, 985 (1959); J. L. Menke, Nucl. Instr. Methods **64**, 61 (1968).

¹²L. I. Schiff, Phys. Rev. **83**, 252 (1951). The real photons were assumed to be produced in 0.0067 g/cm² of Al and 0.0063 g/cm² of Fe upstream of the ${}^4\text{He}$ gas. The number of real photons incident on the target gas was always less than 3% the number of "virtual photons."

¹³F. Mandl, *Quantum Mechanics* (Butterworths Scientific Publications, London, 1954), p. 144.

¹⁴B. Bosco and P. Quarati, Nuovo Cimento **33**, 527 (1964).

¹⁵The relation of the multipole operators defined in Ref. 5 to the usual multipole operators defined in terms of the irreducible representation of the rotation group is given in B. F. Gibson and T. W. Williams, Nucl. Phys. **A163**, 193 (1971).

¹⁶L. I. Schiff, Phys. Rev. **96**, 765 (1954).

¹⁷P. Quarati, Nucl. Phys. **A115**, 681 (1958).

¹⁸M. Gell-Mann and V. L. Telegdi, Phys. Rev. **91**, 169 (1953).

¹⁹J. J. Murphy, II, private communication to W. R. Dodge.

²⁰B. H. Flowers and F. Mandl, Proc. Roy. Soc. (London) **A206**, 131 (1951).

²¹L. M. Delves, Australian J. Phys. **15**, 59 (1962).

²²R. W. Zurmühle, W. E. Stephens, and H. W. Staub, Phys. Rev. **132**, 751 (1963).

²³J. Asbury and F. Loeffler, Phys. Rev. **137**, B124 (1965).

²⁴E. Ahmed, S. M. M. R. Chowdhury, and D. Husain,

Nucl. Phys. **A141**, 664 (1970).

²⁵D. R. Thompson, Nucl. Phys. **A154**, 442 (1970). Our data have been used with our permission in this paper. Unfortunately, the cross-section data we supplied Professor Thompson were too large by a factor of approximately 0.6.

²⁶B. F. Gibson, private communication.

²⁷D. R. Thompson, Nucl. Phys. **A143**, 304 (1970).

²⁸A. B. Volkov, Nucl. Phys. **74**, 33 (1965).

²⁹These curves were calculated by Dr. J. J. Murphy, II.

³⁰A. N. Gorbunov and V. M. Spiridonov, Zh. Eksperim. i Teor. Fiz. **34**, 862 (1958) [transl.: Soviet Phys.-JETP **7**, 596 (1958)].

PHYSICAL REVIEW C

VOLUME 6, NUMBER 1

JULY 1972

Giant Resonances in C^{12}

C. Brassard,* H. D. Shay, J. P. Coffin,† W. Scholz,§ and D. A. Bromley

A. W. Wright Nuclear Structure Laboratory, Yale University, New Haven, Connecticut 06520

(Received 15 November 1971)

Detailed measurements on the reaction $\text{B}^{11}(p, \gamma)\text{C}^{12}$ are reported in the incident proton energy range $14 \leq E_p \leq 22$ MeV. Previously reported absolute cross sections for this reaction have been found to be in question. Measurements have been made leading to the first (2^+) and third (3^-) states of C^{12} in addition to the ground state. No evidence has been found for the predicted resonance at $E_x = 35$ MeV, also reported in earlier experimental work. Detailed calculations based on the one-particle-one-hole model wave functions of Gillet and Vinh-Mau have been compared with the experimental data using a complete R -matrix formalism. Repetition of these calculations using pure j - j configurations yields comparable agreement. Evidence for the importance of many-particle-many-hole configurations in the radiative capture process has been found, particularly in the reaction leading to the first and third excited states, but also in the ground-state reaction data. The calculations are significant in the sense that no new parameters are introduced, nor are any significant approximations used which are not already in the model wave functions under test. The isospin mixing in C^{12} is found to be very small, if the new absolute (p, γ_0) cross section reported here is used; this is in marked contrast to earlier estimates of this mixing.

I. INTRODUCTION

The radiative capture of protons by B^{11} is one of the most extensively studied nuclear reactions¹⁻⁴; however, reliable data were until recently limited to incident proton energies below 14 MeV (shortly after completion of the experiment reported herein, Kernel and Mason extended the measurements to 21 MeV). This continuing interest in the detailed study of the interaction of γ radiation with nuclear matter reflects the relative simplicity of nuclear processes involving electromagnetic radiation. The relative weakness of the electromagnetic forces and our detailed knowledge of them permit the direct testing of nuclear wave functions, with minimal additional approximations. Furthermore, detailed model wave functions of highly excited states reached in these studies have only recently become available; these wave functions can be tested directly in calculations directed toward reproduction of radiative capture experimental results in the appropriate energy region.

C^{12} constitutes an especially interesting com-

pound nucleus for study through radiative capture reactions, since its widely spaced low-lying levels permit the resolution of the radiative transitions to the first four states,⁵ as pictured in Fig. 1, and since extensive information is already available on the structure of the lower-lying excited-state wave functions. Such knowledge is essential to any detailed study of the higher levels. Only the transitions to the ground state and first excited state had been reported previously. In the studies to be reported herein we have measured angular distributions for the reaction $\text{B}^{11}(p, \gamma)\text{C}^{12}$ in the range from 14- to 22-MeV incident proton energy for the γ_0 , γ_1 , and γ_3 transitions; the γ_2 transition to the 7.65-MeV state is weak, and only an upper limit was obtained for the corresponding cross section.

The theoretical interest in the radiative proton capture experiments lies in the fact that the capture cross sections can be calculated directly from the detailed wave functions of the nucleus, without additional assumptions concerning either the reaction mechanism or the structure of the